Robustly protected carrier spin relaxation in electrostatically doped transition-metal dichalcogenides

Zhang, Y. J.; Shi, W.; Ye, J. T.; Suzuki, R.; Iwasa, Y.

Published in:
Physical Review. B: Condensed Matter and Materials Physics

DOI:
10.1103/PhysRevB.95.205302

Publication date:
2017

Robustly protected carrier spin relaxation in electrostatically doped transition-metal dichalcogenides

Y. J. Zhang,[1,2,3] W. Shi,[4] J. T. Ye,[5] R. Suzuki,[1] and Y. Iwasa[1,6]

[1]*Department of Applied Physics and Quantum-Phase Electronics Center (QPEC), The University of Tokyo, 7-3-1 Hongo, Bunkyo, Tokyo 113-8656, Japan*

[2]*The Institute of Scientific and Industrial Research, Osaka University, 8-1, Mihogaoka, Ibaraki, Osaka 067-0047, Japan*

[3]*Max-Planck-Institut für Festkörperforschung, Heisenbergstrasse 1, D-70569 Stuttgart, Germany*

[4]*Materials Sciences Division, Lawrence Berkeley National Laboratory, Berkeley, California 94720, USA*

[5]*Device Physics of Complex Materials, Zernike Institute for Advanced Materials, Nijenborgh 4, 9747 AG, Groningen, Netherlands*

[6]*Center for Emergent Matter Science (CEMS), RIKEN, Wako 351-0198, Japan*

(Received 12 July 2016; published 5 May 2017)

Transition-metal dichalcogenides are unique semiconductors because of their exclusive coupling between the spin and the valley degrees of freedom. The spin flip simultaneously requires a large amount of the crystal momentum variation; hence most of the carrier scattering is expected to be the spin-conserving intravalley scattering. Analysis of the quantum interference effects on the magnetoconductivity in WSe_2, $MoSe_2$, and MoS_2 reveals that the spin-relaxation time is orders of magnitude longer than the carrier momentum scattering time, indicating that the valley-spin coupling robustly protects the spin polarization from carrier scatterings. In addition, the electron-spin-relaxation time of $MoSe_2$ is found to be anomalously short compared to other members, which is likely the origin of the ultrafast valley scattering of excitons in $MoSe_2$.

DOI: 10.1103/PhysRevB.95.205302

I. INTRODUCTION

Electrons and holes in 2H-type group-VIB transition-metal dichalcogenides (TMDs) are unique two-dimensional carriers in which the spin degree of freedom, **s**, is independent of the carrier velocity, **v**, that is proportional to the momentum derivative of the band dispersion, $\partial\varepsilon(\mathbf{k})/\partial\mathbf{k}$. In conventional two-dimensional (2D) carriers, the spin-orbit interaction (SOI) couples **s** and **v**, such as those formed at the interface of III-V binary compounds, where all carrier scattering could lead to the spin relaxation [1]. In marked contrast, SOI in TMDs couples **s** to the crystal momentum, $\hbar\mathbf{k}$, instead of **v**, owing to the broken inversion symmetry in the honeycomb lattice structure of the individual layer [2] as well as the fact that Fermi pockets, which are usually referred to as valleys, are away from the Γ point [3]. The broken inversion symmetry split valleys at six hexagonal Brillouin zone corners into two groups, denoted by $\pm K$, generating a so-called valley degree of freedom. The time-reversal symmetry dictates valley-dependent spin polarization, namely, all carriers in $K(-K)$ valleys should have spin ↑ (↓), which has been experimentally verified by the spin- and angle-resolved photoemission spectroscopy [4,5]. Because of this valley-coupled spin texture, the spin relaxation in TMDs must accompany valley relaxation that requires a large variation of $\hbar\mathbf{k}$. Therefore, the spin relaxation in TMDs is expected to be slow and protected against the carrier scattering.

Experimental studies on the spin and valley relaxation in TMDs have been, so far, limited to optical techniques, which is based on the exclusive coupling between the valley degree of freedom ($\pm K$) and the circular polarization of light ($\sigma_\pm$) [2]. This feature enables optical generation and detection of the valley polarization [6–8], and also realizes valleytronic functional devices [9,10]. Since the optical process generates both electrons and holes simultaneously, the exchange interaction makes the spin and valley relaxation faster than the cases where only a single type of carrier exists [8]. The observation of the spin Hall effect and/or the valley Hall effect [10,11], therefore, requires a sufficiently large electric field to break the excitons into free carriers. To design spintronic and valleytronic devices, reliable estimations of the spin and valley relaxation times of free electrons and holes are highly demanded.

Recently, the spin-relaxation time of free electrons in MoS_2 was investigated by analyzing the quantum interference in the magnetoconductivity [12]. The spin-orbit splitting in the conduction band is relatively small (1−40 meV) so that intravalley electron-spin relaxation is available [13]. On the other hand, the splitting in the valence band is much larger (150−450 meV) and therefore longer spin-relaxation time is expected for holes by largely suppressing the intravalley spin relaxation.

Here, we systematically investigated the spin-relaxation time of electrons and holes in three TMD compounds: WSe_2, $MoSe_2$, and MoS_2, under various free carrier densities controlled by the field-effect transistor (FET) device structure. We revealed that the spin relaxation is largely suppressed compared to the total carrier scattering, particularly in the valence band. In addition, the electron-spin relaxation rate in $MoSe_2$ is found to be anomalously large compared to MoS_2 and WSe_2. As the quantum interference appears only at low temperature, the channel resistances must remain finite down to a sufficiently low temperature. In contrast to MoS_2 [12], metallic states of WSe_2 and $MoSe_2$ are only reachable with liquid gate dielectrics, that have larger carrier accumulation capability [14,15]. In this study, therefore, an ionic liquid (DEME-TFSI) is selected for the gate dielectric [16]. See the Supplemental Material [17] for detailed descriptions and the basic device characterizations. The spin-relaxation time was deduced by analyzing the weak localization (WL) and weak antilocalization (WAL) features in magnetoconductivity at 2 K [Fig. 1(a)]. The Hall effect was also simultaneously measured, from which carrier density n_{2D} and carrier mobility

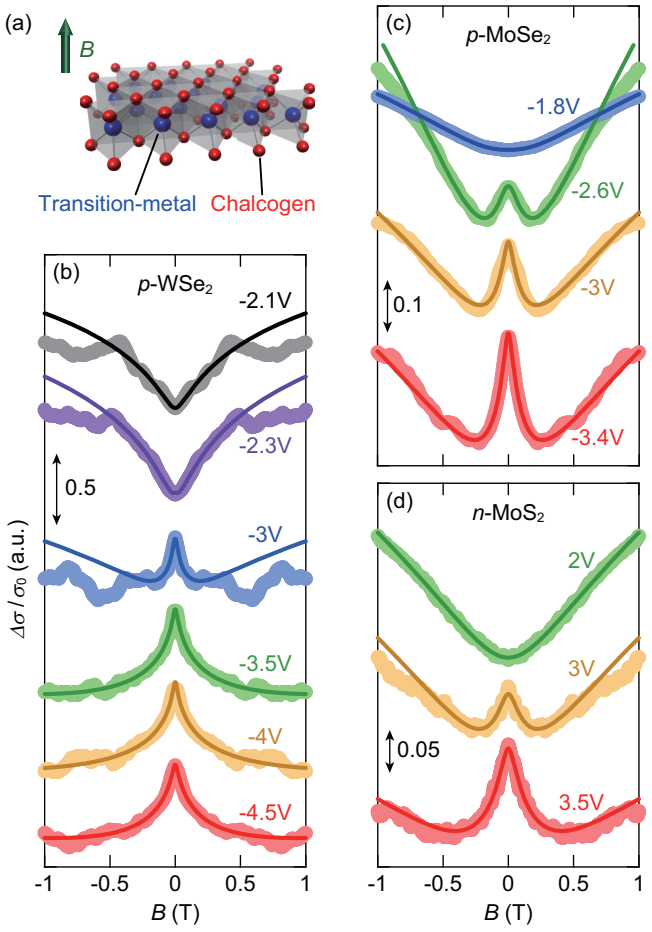

FIG. 1. (a) Schematics of magnetoconductance measurement. (b–d) Gate-voltage dependence of magnetoconductivity of hole-doped WSe_2 (b), hole-doped $MoSe_2$ (c), and electron-doped MoS_2 (d). Shaded lines and solid lines represent experimental data and the fits to the theory, respectively. All measurements were done at 2 K. $\sigma_0 \equiv e^2/\pi\hbar$.

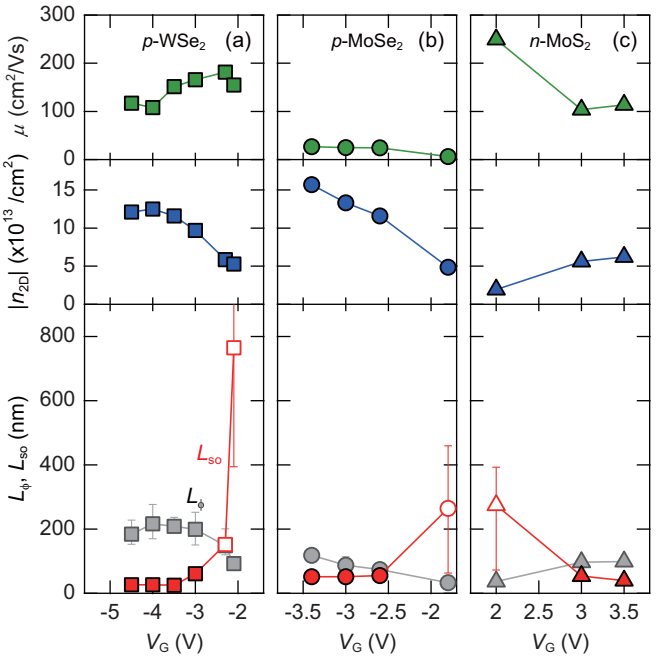

FIG. 2. Comparison of the carrier mobility μ, the carrier density $|n_{2D}|$, the phase coherence length L_ϕ, and the spin-relaxation length L_{so} in hole-doped WSe_2 (a), hole-doped $MoSe_2$ (b), and electron-doped MoS_2 (c), under various gate voltages. Solid and open symbols represent the spin-relaxation length deduced from the fits of the WAL and the WL features, respectively.

μ were deduced. We note that multilayers ahre incorporated in this study. However, valleytronic properties still manifest themselves in the measurement, since $\pm K$ valleys in ion-gated multilayer are occupied, which is experimentally confirmed by electroluminescence measurement [9,18]; additionally, the inversion symmetry is broken by the strong gate electric field [14].

II. MAGNETOTRANSPORT MEASUREMENT AND QUANTUM INTERFERENCE

Figures 1(b)–1(d) display magnetoconductivity at various gatevoltages, V_G. All data were symmetrized to remove possible contribution from the Hall effect. The positive and negative sign of V_G indicates electron and hole doping, respectively, and a larger value of $|V_G|$ implies higher carrier density, $|n_{2D}|$. The quantum interference is recognized by the peak behavior around zero magnetic field, $B = 0$ T. Positive ($\partial\sigma/\partial B > 0$) and negative ($\partial\sigma/\partial B < 0$) magnetoconductivity, respectively, represents WL and WAL. A crossover from WL to WAL was most clearly observed in p-WSe_2 [Fig. 1(b)], which is consistent with previous work on an ion-gated bulk WSe_2 single crystal [14]. Not only p-WSe_2, but also p-$MoSe_2$ [Fig. 1(c)] and n-MoS_2 [Fig. 1(d)] exhibit similar crossover from WL to WAL. In p-$MoSe_2$, a positive magnetoconductivity (WL) appears following the suppression of WAL, but such a positive magnetoconductivity is absent in p-WSe_2 [Fig. 1(b)]. It is known that the general magnetoresistance can overwhelm the WL effect [19]. Figure 2 shows that μ in p-WSe_2 is one order of magnitude higher than that in p-$MoSe_2$, indicating a possibly larger magnetoresistance effect in p-WSe_2.

Magnetoconductivity was analyzed by fitting experimental data with the Hikami-Larkin-Nagaoka theory (HLN theory) [12,20,21]:

$$\sigma(B) - \sigma(0) = \frac{e^2}{2\pi^2\hbar}\left[F\left(\frac{B_\phi + B_{so}}{B}\right) + \frac{1}{2}F\left(\frac{B_\phi + 2B_{so}}{B}\right) - \frac{1}{2}F\left(\frac{B_\phi}{B}\right)\right],$$

with $F(x) \equiv \psi(x + 1/2) - \ln x$, where ψ is the digamma function. B_ϕ and B_{so} are fitting parameters characterizing phase coherence and spin relaxation, respectively. The best fit curves are overplotted in Fig. 1 with solid lines. The discrepancy between the experimental data and the fit becomes larger with increasing $|B|$, because the theoretical formula does not include conventional magnetoresistance scaling with B^2. Therefore, a cutoff magnetic field was set during the fit. By changing the cutoff magnetic field, the results of the fit differ slightly, as indicated by error bars in Figs. 2 and 3. During analysis, we followed Schmidt *et al.* [12] to fit all experimental data with the identical formula including both B_ϕ and B_{so}. The

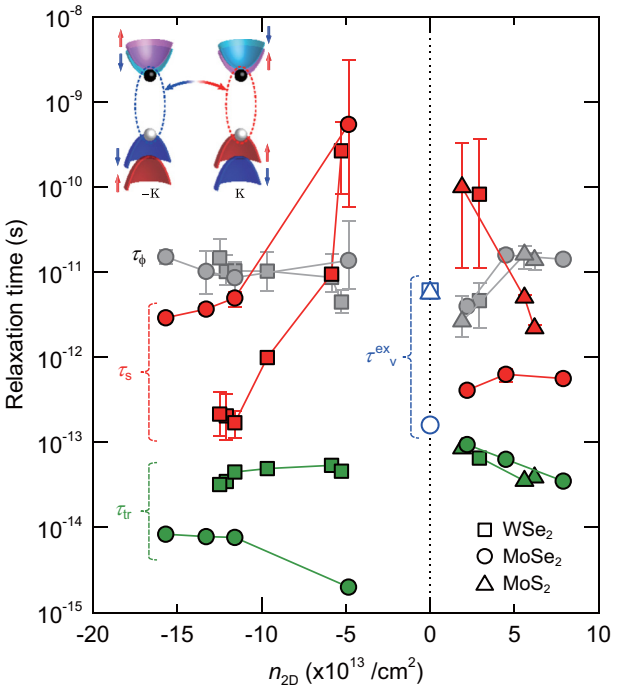

FIG. 3. Carrier density dependence of the spin-relaxation time τ_s, the phase coherence time τ_ϕ, and the momentum scarring time τ_{tr}. The valley life time τ_v^{ex} of exciton is overplotted at $n_{2D} = 0$. The inset shows the schematic band structure around $\pm K$ valleys.

fittings agree reasonably well with the experimental data, but care must be taken because B_{so} values deduced from WL are less reliable than those deduced from WAL. The variation of B_{so} does not significantly affect the overall feature of WL if $B_{so} < B_\phi$ [22].

Using the relation $L_\alpha^2 = \hbar/(4eB_\alpha)$ ($\alpha = \phi$, so), B_ϕ and B_{so} are converted to the phase coherence length L_ϕ, and the spin-relaxation length L_{so}, respectively. Filled and open symbols in Fig. 2 represent L_{so} deduced from magnetoconductivity showing WAL and WL, respectively. The lower reliability of L_{so} in the WL region is evident by the larger error bars. The crossover from WL to WAL occurs when $L_\phi \approx L_{so}$. WL is seen when the carrier spin relaxation is less frequent than the carrier phase relaxation so that spin components can be ignored when considering the standing wave along closed carrier motion paths [23]. On the other hand, when the spin relaxation becomes more frequent than the phase relaxation, the spin component of the wave function can suppress the standing wave formation, leading to WAL.

III. DISCUSSION

A. Spin-relaxation time in electrostatically doped TMDs

To clarify the difference between scatterings of the carrier phase, the carrier spin, and the carrier momentum, the spin-relaxation time, $\tau_s = L_{so}^2/D$, the phase coherence time, $\tau_\phi = L_\phi^2/D$, and the momentum scattering time, $\tau_{tr} = \mu m^*/q$, were estimated. Here D, m^*, and q represent the diffusion constant, the effective carrier mass, and the elementary charge, respectively. In a manner similar to the relation between L_ϕ and L_{so}, τ_s is shorter (longer) than τ_ϕ in the WAL (WL) regime (Fig. 3). When the electron density is reduced to $n_{2D} \sim 2 \times 10^{13}/\text{cm}^2$, τ_s for n-MoS_2 reaches the order of 10 ps, being consistent with the reported value [12]. On the other hand, the relation between τ_s and τ_{tr} is inconsistent with Ref. [12]. This discrepancy may possibly be attributed to the difference of the carrier density regimes investigated. The carrier density region in Ref. [12] is $1-2 \times 10^{13}/\text{cm}^2$, while we varied the carrier density from $\sim 10^{13}$ to $\sim 10^{14}/\text{cm}^2$. Only one data point from our study locates in the carrier density region investigated in Ref. [12]. As the band structure changes with the carrier density [24,25], the dominant spin-relaxation mechanism may also change. The difference in layer numbers is also expected to contribute to this discrepancy. We further note that the theoretical work is not sufficient at the present stage. Since the HLN theory only takes the Elliott-Yafet (EY) mechanism into account [20], a theoretical study with the Dyakonov-Perel (DP) mechanism, which is the claim of Ref. [12], is highly required before the detailed argument of the spin-relaxation mechanism.

The decrease of τ_s with the increasing $|n_{2D}|$ in Fig. 3 indicates that the spin relaxation can be controlled by FET devices, which may be attributed to two facts. Firstly, FET devices modify the effective magnetic field, B_{eff}. The variation of $|n_{2D}|$ indicates not only the variation of the Fermi energy but also the variation of the perpendicular electric field E_p, applied at TMD surfaces through the gate voltage. Carriers feel B_{eff} when an electric field is applied perpendicular to their momentum. The broken inversion symmetry of TMD crystal structure generates an out-of-plane B_{eff} that leads to a huge spin splitting around $\pm K$ valleys [2]. Additionally, E_p generates an in-plane B_{eff} since carrier motion is limited to in plane. This is similar to the well-known Rashba effect [1]. Although this in-plane B_{eff} is orders of magnitude smaller than the out-of-plane B_{eff}, the in-plane B_{eff} could assist the spin flip, which is required for the intervalley scattering, by inducing Larmor precession.

Secondly, the band structure is modified with doping, and different types of valleys are simultaneously occupied. Monolayers and multilayers of TMDs differ from each other in terms of electronic structure. The bottom of the conduction band locates at $\pm K$ points in monolayers, and at $\pm T$ points ($\pm Q$ points) in multilayers. However, theoretical works predicted that under high carrier density, both the $\pm K$ and the $\pm T$ valleys of the conduction band are occupied in both monolayers [24] and multilayers [25]. In case of the valence band, the $\pm K$ valleys and the Γ valley can be simultaneously occupied. In these situations, the carrier scattering between different types of valleys can enhance the total carrier scattering and the spin scattering, making our estimation as a lower bound since the pure spin-relaxation time between $\pm K$ valleys could be even longer.

B. Comparison of spin relaxation of electrostatically doped carriers in TMDs and other semiconductors

Modification of τ_s by tuning the electric field and thus carrier density in the FET device structure is well known for various semiconductors [26,27]. In Fig. 4(a), we compare τ_s and τ_{tr} of TMDs with those of the AlGaAs quantum well (QW) [26] and $LaAlO_3/SrTiO_3$ (LAO/STO) heterostructure

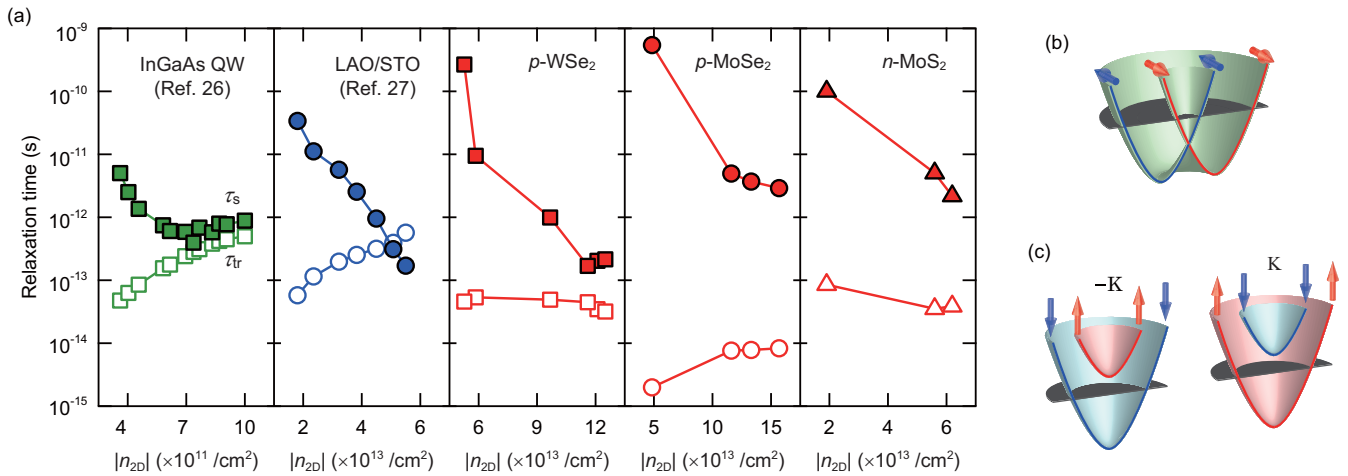

FIG. 4. (a) Comparison of spin- (filled symbols) and momentum- (open symbols) relaxation times in conventional semiconductor and TMDs. Data of InGaAs QW and LAO/STO are taken from Refs. [26,27], respectively. (b) Schematic band dispersions of Rashba system. (c) Schematic band dispersions of valley-spin locking in TMDs.

[27]. Basically, all materials show the decrease of τ_s with increasing carrier density. Importantly, when one looks at the lowest carrier density data point, τ_s's of TMDs are larger than the AlGaAs QW and LAO/STO even though τ_{tr}'s are shorter in TMDs. As these values strongly depend on the sample quality, we took the ratio $R_\tau \equiv \tau_s/\tau_{tr}$ as a material-specific parameter. R_τ can be interpreted as the amount of carrier momentum scatterings required to flip spin once, and $1/R_\tau$ represents the spin-flip probability among the single carrier momentum scattering. Figure 4(a) clearly shows that R_τ becomes larger when the carrier density is smaller. In Table I, the maximum R_τ's in each material are compared. The R_τ's of TMDs are quite large, especially in the valence band, indicating that the spin is highly protected against the carrier scattering. These values are even orders of magnitude larger than those of conventional 2D carriers [26,27]. In Rashba systems $\mathbf{s}$ and $\mathbf{v}[\partial\varepsilon(\mathbf{k})/\partial\mathbf{k}]$ are coupled [Fig. 4(b)] and every carrier scattering accompanies spin relaxation to some extent. The spin-helical mode and the persistent spin helix is one of the possible solutions to realize carrier velocity-independent spin polarization [28]. On the other hand, the SOI-induced effective magnetic field in TMDs is almost independent from $\mathbf{v}$ and only depends on the valley degree of freedom required by the symmetry of TMDs [Fig. 4(c)] [5]. Since the intervalley scattering requires a large $\hbar\mathbf{k}$ variation and a simultaneous spin flip, the carrier scattering is expected to be dominated by the spin-conserved intravalley scattering with less $\hbar\mathbf{k}$ variation. Therefore, the spin is protected against the total carrier scattering, which is evident by the larger values of R_τ, especially for holes with a larger spin splitting (Table I).

We note that $R_\tau \approx 10^3$ is reported in conventional semiconductor QWs measured with optical technique [29,30], but in Fig. 4(a) and Table I we focused on R_τ's obtained from magnetoconductance measurement for comparison with our results. The optical method is advantageous for the measurements in the low carrier density regime, which is difficult to access by transport measurements. The carrier density in Refs. [29,30] is smaller than that in Ref. [26]. Following the trend of τ_s and τ_{tr} in Fig. 3, it is likely that R_τ in TMDs could be further enhanced in the lower carrier density regime. This trend is theoretically predicted in hole-doped TMDs [31]. Also, a larger τ_s of 3 ns was reported in naturally doped (very lightly doped) n-MoS_2 and n-WS_2 [32].

TABLE I. A summary table of the maximum value of R_τ in TMDs and Rashba systems. The spin-relaxation time and the momentum scattering time which give the maximum R_τ are also listed.

Material	Max R_τ	τ_s (ps)	τ_{tr} (ps)
p-WSe_2	5.9×10^3	2.7×10^2	0.046
n-WSe_2	1.3×10^3	82	0.065
p-$MoSe_2$	2.7×10^5	5.5×10^2	0.0020
n-$MoSe_2$	4.4	0.41	0.094
n-MoS_2	1.2×10^3	1.0×10^2	0.085
InGaAs QW[a]	1.0×10^2	5.0	0.048
LAO/STO[b]	5.9×10^2	34	0.058

[a]Reference [28].
[b]Reference [29].

C. Anomalously fast spin relaxation of electrons in $MoSe_2$

So far, the overall feature of τ_s in TMDs is compared with that in the Rashba system. On the other hand, a detailed comparison of τ_s between various TMD members clarifies that τ_s in n-$MoSe_2$ is kept small and almost independent of n_{2D} in the whole positive n_{2D} region (Fig. 3). The small τ_s in n-$MoSe_2$ is also evident from the WAL feature [17]. Such an anomalously small τ_s is expected to be intrinsic to $MoSe_2$ because of the following two reasons. First, τ_{tr} are similar in three materials, indicating that the particular $MoSe_2$ device is similar in sample quality to the other two devices of WSe_2 and MoS_2. Second, the identical $MoSe_2$ device clearly shows modulation of τ_s for holes, implying that the FET device is properly working in applying E_p to the channel.

The anomalously short τ_s in $MoSe_2$ reminds us of the negligibly small circular polarization in photoluminescence (PL) from $MoSe_2$, which is attributed to the ultrafast valley relaxation of excitons in $MoSe_2$ [33]. The degree of circular polarization in time-integrated PL, η, is determined by the exciton life time, τ^{ex}, and the exciton valley relaxation time, τ_v^{ex}, within a rate equation framework [34]. Prior studies using time-resolved PL techniques identified that τ^{ex} at liquid-helium temperature is independent of the materials composition and is around 4 ps [33,35,36]. On the other hand, τ_v^{ex} is only known for WSe_2 ($\sim$6 ps) investigated by time-resolved Kerr rotation measurement [37], being similar to τ^{ex}. Following the rate equation [34], these values predict $\eta \approx 60\%$, which is consistent with the experimentally observed value for WSe_2 [38]. Therefore, it is a reasonable way to estimate τ_v^{ex} in other compounds by combining the rate equation with τ^{ex} and η.

Comparison between τ_v^{ex} and τ_s should be fruitful, since the exciton valley relaxation is related to electron- and hole-spin relaxation (see illustration in Fig. 3). τ_v^{ex} values of various TMD members are overplotted in Fig. 3 at $n_{2D} = 0$ with blue symbols. The filled and open symbols represent the direct experimental value and the calculated value, respectively. The reduction from τ_s to τ_v^{ex} can be mainly attributed to the exchange interaction [8]. Figure 3 indicates that the ultrafast exciton valley relaxation in $MoSe_2$ can be attributed to the fast electron-spin relaxation, although further studies are required to clarify the underlying mechanism of the anomalously fast electron-spin relaxation in $MoSe_2$.

IV. CONCLUSIONS

In summary, we have made a systematic study of the magnetoconductance at 2 K in the gate-induced conducting states of TMDs. The carrier spins in TMDs are found to be robustly protected against carrier scatterings, owing to the independency between the spin degree of freedom and the carrier velocity. The spin relaxation can be triggered and controlled in a large range by external electric field. We further found that n-$MoSe_2$ has anomalously short spin-relaxation time, which is likely the origin of unpolarized PL.

ACKNOWLEDGMENTS

We thank M. Kohda for fruitful discussions. Y.J.Z. and R.S. are supported by Japan Society for the Promotion of Science (JSPS) through the research fellowship for young scientists. R.S. is also supported by Materials Education program for the future leaders in Research, Industry, and Technology (MERIT). J.T.Y. acknowledges funding from the European Research Council (consolidator Grant No. 648855 Ig-QPD). This research was supported by Grant-in-Aid for Specially Promoted Research (Grant No. 25000003) from JSPS.

[1] I. Žutić, J. Fabian, and S. Das Sama, Rev. Mod. Phys. **76**, 323 (2004).
[2] D. Xiao, G. B. Liu, W. Feng, X. Xu, and W. Yao, Phys. Rev. Lett. **108**, 196802 (2012).
[3] Y. Song and H. Dery, Phys. Rev. Lett. **111**, 026601 (2013).
[4] R. Suzuki, M. Sakano, Y. J. Zhang, R. Akashi, D. Morikawa, A. Harasawa, K. Yaji, K. Miyamoto, T. Okuda, K. Ishizaka, R. Arita, and Y. Iwasa, Nat. Nanotechnol. **9**, 611 (2014).
[5] J. M. Riley, F. Mazzola, M. Dendzik, M. Michiardi, T. Takayama, L. Bawden, C. Granerød, M. Leandersson, T. Balasubramanian, M. Hoesch, T. K. Kim, H. Takagi, W. Meevasana, P. Hofmann, M. S. Bahramy, J. W. Wells, and P. D. C. King, Nat. Phys. **10**, 835 (2014).
[6] T. Cao, G. Wang, W. P. Han, H. Q. Ye, C. R. Zhu, J. R. Shi, Q. Niu, P. H. Tan, E. Wang, B. L. Liu, and J. Feng, Nat. Commun. **3**, 887 (2012).
[7] H. Zeng, J. Dai, W. Yao, D. Xiao, and X. Cui, Nat. Nanotechnol. **7**, 490 (2012).
[8] K. F. Mak, K. He, J. Shang, and T. F. Heinz, Nat. Nanotechnol. **7**, 494 (2012).
[9] Y. J. Zhang, T. Oka, R. Suzuki, J. T. Ye, and Y. Iwasa, Science **344**, 725 (2014).
[10] K. F. Mak, K. L. McGill, J. Park, and P. L. McEuen, Science **344**, 1489 (2014).
[11] X. Li, F. Zhang, and Q. Niu, Phys. Rev. Lett. **110**, 066803 (2013).
[12] H. Schmidt, I. Yudhistira, L. Chu, A. H. Castro Neto, B. Özyilmaz, S. Adam, and G. Eda, Phys. Rev. Lett. **116**, 046803 (2016).
[13] G.-B. Liu, W.-Y. Shan, Y. Yao, W. Yao, and D. Xiao, Phys. Rev. B **88**, 085433 (2013).
[14] H. T. Yuan, M. S. Bahramy, K. Morimoto, S. F. Wu, K. Nomura, B.-J. Yang, H. Shimotani, R. Suzuki, M. Toh, C. Kloc, X. D. Xu, R. Arita, N. Nagaosa, and Y. Iwasa, Nat. Phys. **9**, 563 (2013).
[15] W. Shi, J. T. Ye, Y. J. Zhang, R. Suzuki, M. Yoshida, J. Miyazaki, N. Inoue, Y. Saito, and Y. Iwasa, Sci. Rep. **5**, 12534 (2015).
[16] Y. J. Zhang, J. T. Ye, Y. Matsuhashi, and Y. Iwasa, Nano Lett. **12**, 1136 (2012).
[17] See Supplemental Material at http://link.aps.org/supplemental/10.1103/PhysRevB.95.205302 for experimental methods, device characterizations, and additional magnetoresistance data.
[18] S. Jo, N. Ubrig, H. Berger, A. B. Kuzmenko, and A. F. Morpurgo, Nano Lett. **14**, 2019 (2014).
[19] V. A. Guzenko, T. Schäpers, and H. Hardtdegen, Phys. Rev. B **76**, 165301 (2007).
[20] S. Hikami, A. I. Larkin, and Y. Nagaoka, Prog. Theor. Phys. **63**, 707 (1980).
[21] S. V. Iordanskii, Yu. B. Lyanda-Geller, and G. E. Pikus, Pis'ma Zh. Eksp. Teor. Fiz. **60**, 199 (1994) [JETP Lett. **60**, 206 (1994)].
[22] F. V. Tikhonenko, A. A. Kozikov, A. K. Savchenko, and R. V. Gorbachev, Phys. Rev. Lett. **103**, 226801 (2009).
[23] G. Bergmann, Phys. Rep. **107**, 1 (1984).
[24] Y. Ge and A. Y. Liu, Phys. Rev. B **87**, 241408(R) (2013).
[25] T. Brumme, M. Calandra, and F. Mauri, Phys. Rev. B **91**, 155436 (2015).
[26] T. Koga, J. Nitta, T. Akazaki, and H. Takayanagi, Physica E **13**, 542 (2002).
[27] A. D. Caviglia, M. Gabay, S. Gariglio, N. Reyren, C. Cancellieri, and J.-M. Triscone, Phys. Rev. Lett. **104**, 126803 (2010).

[28] J. D. Koralek, C. P. Weber, J. Orenstein, B. A. Bernevig, S.-C. Zhang, S. Mack, and D. D. Awschalom, Nature **458**, 610 (2009).
[29] T. Korn, M. Kugler, M. Griesbeck, R. Schulz, A. Wagner, M. Hirmer, C. Gerl, D. Schuh, W. Wegscheider, and C. Schüller, New J. Phys. **12**, 043003 (2010).
[30] R. Völkl, M. Schwemmer, M. Griesbeck, S. A. Tarasenko, D. Schuh, W. Wegscheider, C. Schüller, and T. Korn, Phys. Rev. B **89**, 075424 (2014).
[31] T. Habe and M. Koshino, Phys. Rev. B **93**, 075415 (2016).
[32] L. Yang, N. A. Sinitsyn, W. Chen, J. Yuan, J. Zhang, J. Lou, and S. A. Crooker, Nat. Phys. **11**, 830 (2015).
[33] G. Wang, E. Palleau, T. Amand, S. Tongay, X. Marie, and B. Urbaszek, Appl. Phys. Lett. **106**, 112101 (2015).
[34] G. Kioseoglou, A. T. Hanbicki, M. Currie, A. L. Friedman, D. Gunlycke, and B. T. Jonker, Appl. Phys. Lett. **101**, 221907 (2012).
[35] G. Wang, L. Bouet, D. Lagarde, M. Vidal, A. Balocchi, T. Amand, X. Marie, and B. Urbaszek, Phys. Rev. B **90**, 075413 (2014).
[36] D. Lagarde, L. Bouet, X. Marie, C. R. Zhu, B. L. Liu, T. Amand, P. H. Tan, and B. Urbaszek, Phys. Rev. Lett. **112**, 047401 (2014).
[37] C. R. Zhu, K. Zhang, M. Glazov, B. Urbaszek, T. Amand, Z. W. Ji, B. L. Liu, and X. Marie, Phys. Rev. B **90**, 161302(R) (2014).
[38] A. M. Jones, H. Y. Yu, N. J. Ghimire, S. F. Wu, G. Aivazian, J. S. Ross, B. Zhao, J. Q. Yan, D. G. Mandrus, D. Xiao, W. Yao, and X. D. Xu, Nat. Nanotechnol. **8**, 634 (2013).